Protist, Vol. 161, 264–278, April 2010
http://www.elsevier.de/protis
Published online date 28 December 2009

Protist

ORIGINAL PAPER

Ultrastructure and Molecular Phylogenetic Position of a Novel Phagotrophic Stramenopile from Low Oxygen Environments: *Rictus lutensis* gen. et sp. nov. (Bicosoecida, incertae sedis)

Naoji Yubuki[a,1], Brian S. Leander[a], and Jeffrey D. Silberman[b]

[a]Canadian Institute for Advanced Research, Program in Integrated Microbial Biodiversity, Departments of Botany and Zoology, University of British Columbia, 6270 University Boulevard, Vancouver, BC V6T 1Z4, Canada
[b]Department of Biological Sciences, University of Arkansas, Fayetteville, AR 72701, USA

Submitted July 12, 2009; Accepted October 11, 2009
Monitoring Editor: Michael Melkonian

A novel free free-living phagotrophic flagellate, *Rictus lutensis* gen. et sp. nov., with two heterodynamic flagella, a permanent cytostome and a cytopharynx was isolated from muddy, low oxygen coastal sediments in Cape Cod, MA, USA. We cultivated and characterized this flagellate with transmission electron microscopy, scanning electron microscopy and molecular phylogenetic analyses inferred from small subunit (SSU) rDNA sequences. These data demonstrated that this organism has the key ultrastructural characters of the Bicosoecida, including similar transitional zones and a similar overall flagellar apparatus consisting of an x fiber and an L-shape microtubular root 2 involved in food capture. Although the molecular phylogenetic analyses were concordant with the ultrastructural data in placing *R. lutensis* with the bicosoecid clade, the internal position of this relatively divergent sequence within the clade was not resolved. Therefore, we interpret *R. lutensis* gen. et sp. nov. as a novel bicosoecid incertae sedis.

Key words: Bicosoecida; flagellar apparatus; Placididae; MAST; Stramenopile.

Introduction

Stramenopiles form a robust and diverse clade of eukaryotes, and ultrastructural studies of the flagellar apparatus have been used to characterize major subclades within the group (Andersen 1989, 1991, 2004; Barr and Allan 1985). The flagellar apparatus consists of the flagella, associated basal bodies and a microtubular rootlet system originating from the basal bodies. This apparatus plays an important role in several eukaryotic cell functions, such as anchoring cell organelles, cell locomotion, and the organization of microtubules associated with the mitotic spindle and the superficial cytoskeleton (Moestrup 1982). Investigations of the flagellar apparatus have helped erect lineages such as the Phaeophyceae, Chrysophyceae, Synurophyceae, Raphidophyceae, Xanthophyceae and Oomycota (Andersen 1987, 1989, 1991, 2004). Since the mid-1990's, molecular phylogenetic analyses have

[1]Corresponding author; fax +1 604 822 6089
e-mail yubuki@interchange.ubc.ca (N. Yubuki).

doi:10.1016/j.protis.2009.10.004

also been used to infer evolutionary relationships among various group within the stramenopiles (Andersen et al. 1993; Ben Ali et al. 2002; Daugbjerg and Andersen 1997; Riisberg et al. 2009; Van de Peer et al. 1996).

Morphological and molecular data have also been used to infer that photosynthetic members arose from a common photosynthetic ancestor (Ben Ali et al. 2002; Daugbjerg and Andersen 1997; Riisberg et al. 2009) and that several lineages of heterotrophic stramenopiles diverged prior to origin of extant photosynthetic stramenopiles (Leipe et al. 1994, 1996). However, tracing plastid evolution may be more complicated (Archibald 2009). Heterotrophic stramenopiles are a polyphyletic assemblage with diverse modes of life. Five major subclades of heterotrophic stramenopiles have been established with a combination of morphological characters and molecular phylogenetic analyses: (1) bicosoecids (phagotrophic flagellates) (Karpov et al. 2001), (2) placidideans (phagotrophic flagellates) (Moriya et al. 2002), (3) labyrinthulids (marine slime nets) (Honda et al. 1999; Tsui et al. 2009), (4) *Blastocystis* (parasites in animals) (Arisue et al. 2002; Silberman et al. 1996) and slopalinids (opalinids and proteromonads, parasites in amphibians and reptiles) (Kostka et al. 2004, 2007; Patterson 1985, 1989) and (5) *Developayella* (phagotrophic flagellates) (Leipe et al. 1996; Tong 1995), Oomycetes (water molds), and Hyphochytridiomycetes (Dick 2001; Riisberg et al. 2009).

Because of tiny cell sizes (often <10 μm) and the lack of conspicuous morphological features under the light microscope, it is necessary to study most phagotrophic stramenopiles with electron microscopy. The general ultrastructure, especially the flagellar apparatus, of phagotrophic stramenopiles has been investigated since 1995 when a number of the flagellates were described as novel species in the Bicosoecida or Placidiidea. These lineages were collected from diverse environments including terrestrial soils, tide pools, coastal sediments, the open ocean, deep sea sediments, and solar salterns (Fenchel and Patterson, 1988; Guillou et al. 1999; Karpov 2000; Karpov et al. 1998; Moriya et al. 2000, 2002; O'Kelly and Nerad 1998; O'Kelly and Patterson 1996; Park et al. 2006; Teal et al. 1998; Tong 1995). It is likely that a large number of heterotorophic stramenopiles remain undiscovered from various environments. Moreover, environmental surveys of DNA sequence have demonstrated a large number of unique SSU clades of uncultured/unidentified presumably heterotrophic stramenopiles, such as the MAST clades (i.e., "marine stramenopile" clades) (Behnke et al. 2006; Massana et al. 2004; Takishita et al. 2007). The problem of interpreting phylogenetic analyses from the exclusive use of environmental sequences is that the cellular identities of the sequences are unknown. Comparative studies based on morphological features of stramenopiles are needed to elucidate the cryptic diversity of the heterotrophic stramenopiles that are evident from environmental sequence data.

Accordingly, we successfully established a culture of a novel heterotrophic flagellate isolated from low oxygen marine sediments and characterized this lineage with ultrastructure and molecular phylogenetic analyses inferred from SSU sequences. Our results demonstrated that the isolate described below is a novel bicosoecid (incertae sedis), designated here as *Rictus lutensis* gen. et sp. nov.

Results

General Morphology of *Rictus lutensis* gen. et sp. nov.

Rictus lutensis was 6.8 μm (5.2-8.7 μm) long and 6.0 μm (4.4-8.5 μm) wide (n=32). Cells were spherical to "D"- shaped when observed laterally (Figs 1, 2A). Because *R. lutensis* cells were usually stuck in bacterial aggregates, the cells did not glide on the substrate (like *Caecitellus)* (O'Kelly and Nerad 1998). When the culture vessel was disturbed, the cells were able to swim in the water column in a spiral motion and rotate clockwise when viewed from the anterior end. Two flagella emerged subapically from the ventral side of the cell. Flagellum 1 (F1, posterior flagellum) was three to five times the length of the cell and trailed behind the cell and undulated in a sinuous pattern. Flagellum 2 (F2, anterior flagellum) was one to one and a half times the length of the cell and was held laterally to the left side of the cell. F2 did not extend forward and did not beat in a sinusoidal pattern like the anterior flagellum of a typical swimming cell of stramenopiles; thus the pulling cell pattern and water currents created towards the cell body by the anterior flagellum was not observed. A permanent and prominent cytostome was located on the posterio-ventral side of the cell, and the cytopharynx was positioned on the posterio-ventral side of the cell and continuous with the cytostome (Figs 1B, C, 2A, B). The cytostome and cytopharynx were supported by

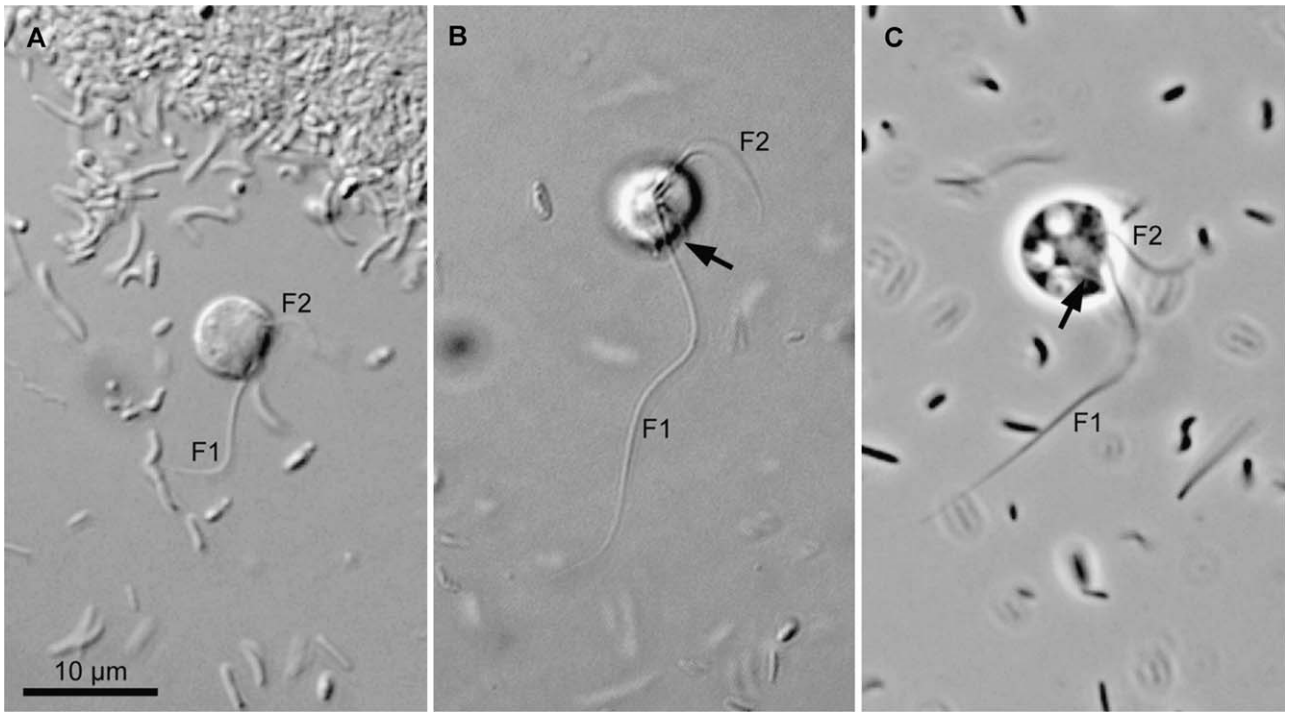

Figure 1. Light micrographs of *Rictus lutensis* gen. et sp. nov. **A**. A living cell with two flagella: flagellum 1 (F1) and flagellum 2 (F2). **B**. A fixed cell focusing on the F1 and cytostome located on posterio-ventral side of the cell (arrow). **C**. A lateral view of a fixed cell showing the cylindrical cytopharynx (arrow) extending inward from the posterio-ventral cytostome.

microtubules consisting of the microtubular root 1 (R1), root 2 (R2) and an S tubule originating from basal body 1 (B1) (Fig. 3A, B; see below for the detail). *R. lutensis* was not a suspension feeder like *Cafeteria* (O'Kelly and Patterson 1996) that forms a feeding cup to ingest food particles; instead, this organism was a raptorial feeder that preyed on bacteria using the permanent cytostome (Fig. 2B) like *Caecitellus* (O'Kelly and Nerad 1998). The nucleus was situated in the subapical region of the cell, close to the flagellar apparatus. The cell possessed two membrane-bounded mitochondria-like organelles (MLO). The MLOs were positioned immediately beneath the cell surface and were filled with a dense matrix and a few swollen cristae (Fig. 3C). The cell surface was not decorated with any structures (e.g., scales or hairs); no indication of a plastid, such as a chloroplast or a leucoplast, was evident; cyst formation or sexual reproduction was not observed.

Flagellar Apparatus

The flagellar apparatus of *Rictus lutensis* was comprehensively characterized at various angles using serial TEM sections. The overall organization of the flagellar root system was consistent with and clearly homologous to the flagellar root system of other stramenopiles. Therefore, we applied the terminology used by Moestrup (2000) to describe the flagellar apparatus in *R. lutensis*.

Flagella and basal bodies: Both F1 and F2 are smooth and no accessory structures, such as hairs or flagellar scales, were present (Fig. 2B, C). However, the flagella did possess acronematic distal tips (Fig. 2A). The basal bodies, B1 and B2, were associated with F1 and F2, respectively. The basal bodies were arranged at a right angle to each other, and B1 was located at the proximal one third of B2. B1 was situated along the longitudinal axis of the cell, and B2 pointed laterally toward the left side of the cell (Fig. 3D, E). Each flagellum connected to its associated basal body via a concave transitional plate (Fig. 3D). Cross sections through the transitional zones demonstrated that the edges of the concave transitional plates formed a concentric ring (Fig. 3F). Neither a transitional helix nor a spiral fiber above or under the transitional plate was observed. Intrakinetosomal shelves were observed in the basal bodies (Fig. 3E). Electron dense material surrounded the proximal end of B1 (Fig. 3G).

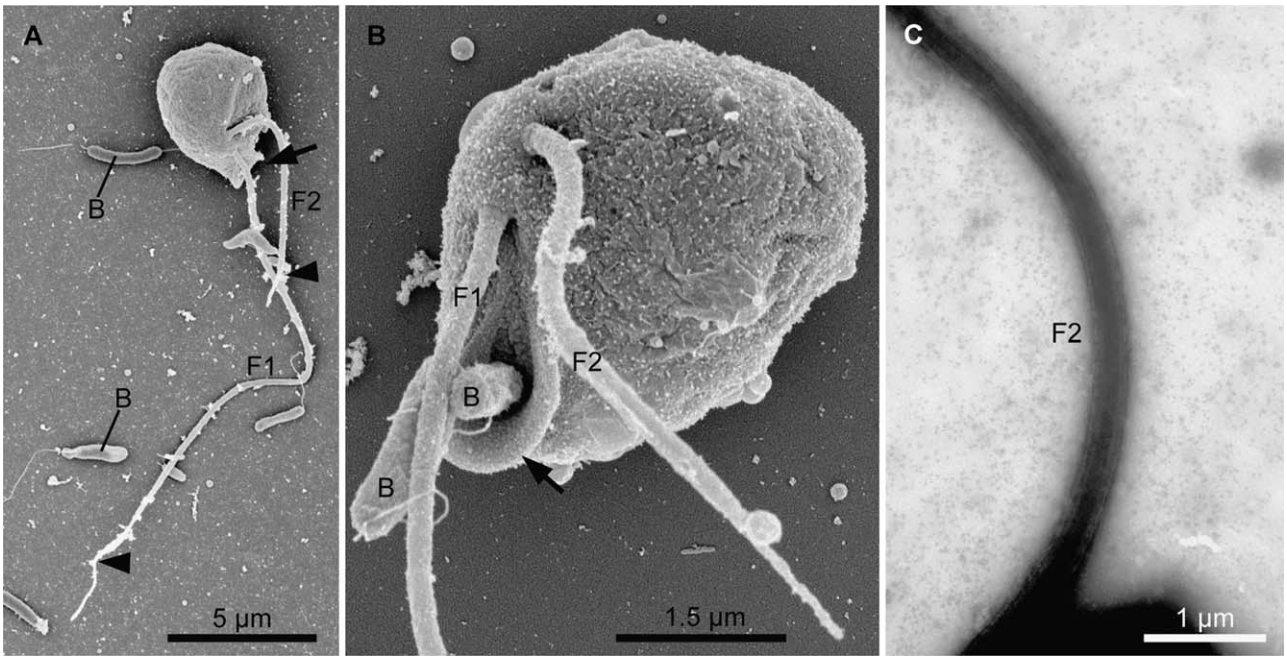

Figure 2. Scanning electron micrographs (A and B) and a negative-stained transmission electron micrograph (C) of *Rictus lutensis* gen. et sp. nov. **A**. Cell with a long posterior flagellum 1 (F1) and a short anterior flagellum 2 (F2). The arrow points to the cytostome and the arrowheads show the distal ends of the acronematic flagella. This cell is viewed from anterior end. **B**. Micrograph showing the absence of hairs or scales on the cell and the flagella. A bacterium (B) is embedded within the cytostome (arrow). This cell is viewed from left side; the cytostome is on the ventral side of the cell. **C**. A high magnification negative-stained TEM of F2 showing the absence of mastigonemes and scales.

Three microtubular roots extended from B1: root 1 (R1), root 2 (R2) and an S tubule (Fig. 4). A single microtubular root, root 3 (R3), originated from B2. The dorsal side of B1, the posterior side of B2, and R2 were all connected by a striated fiber (Fig. 3D, E). Four dense bands extended from B1 and connect with both the S tubule and R2 (Fig. 3H).

Root 1 (R1) and the S tubule (S): R1 consisted of two microtubules and originated from the ventral side of B1, extending toward the left posterior side of the cell. The two microtubules were linked by a fiber (Fig. 4B-I). Only a single microtubule, the S tubule, originated from the dorsal side of B1 and the left side of the 'abc' component of R2. This microtubule extended to the left posterior side and ran in parallel with R1 beneath the cell surface. R1 and the S tubule were linked by a connective band (Fig. 4D-I) and supported the left side of the cytostome. These microtubules terminated prior to the loop structure constructed by R2 (Fig. 4J, K).

Root 2 (R2) and associated structures: R2 was the main supportive structure of the cytostome and cytopharynx (Fig. 5). We applied the labeling system to the root described in Moestrup and Thomsen (1976) ('abc', 'x fiber', etc.). R2 encompassed three main components: (1) three microtubules labeled as 'abc', (2) a single microtubule labeled as the 'x fiber' and (3) an ordered array of additional microtubules (Fig. 4D). At least four microtubules (termed 4, 5, 6 and 7) were located near the origin of R2 at the right posterior side of B1 (Fig. 4A). As R2 extended posteriorly, microtubules were added one by one to the side of microtubule 4 (Fig. 4B) and joined the x-fiber; seven microtubules and the x fiber were aligned in parallel. The 'abc' microtubules joined the left side of microtubule 7. Thus, R2 was L-shaped in cross section: three 'abc' microtubules formed a short arm, and seven microtubules and the x fiber formed a long arm (Fig. 4C). The R2 separated into the 'abc' microtubules and the remaining R2 (Fig. 4D).

The 'abc' microtubules ran posteriorly at a right angle to the cell membrane, and the 'c' microtubule was closest to the membrane. An electron dense fiber was located on the right side of the 'abc' microtubules (Fig. 4D, E). A sheet structure extended from the 'a' microtubule into the cell (Fig. 4E-H), and a thin layer extended from the 'c' microtubule to the left side of the cell just beneath

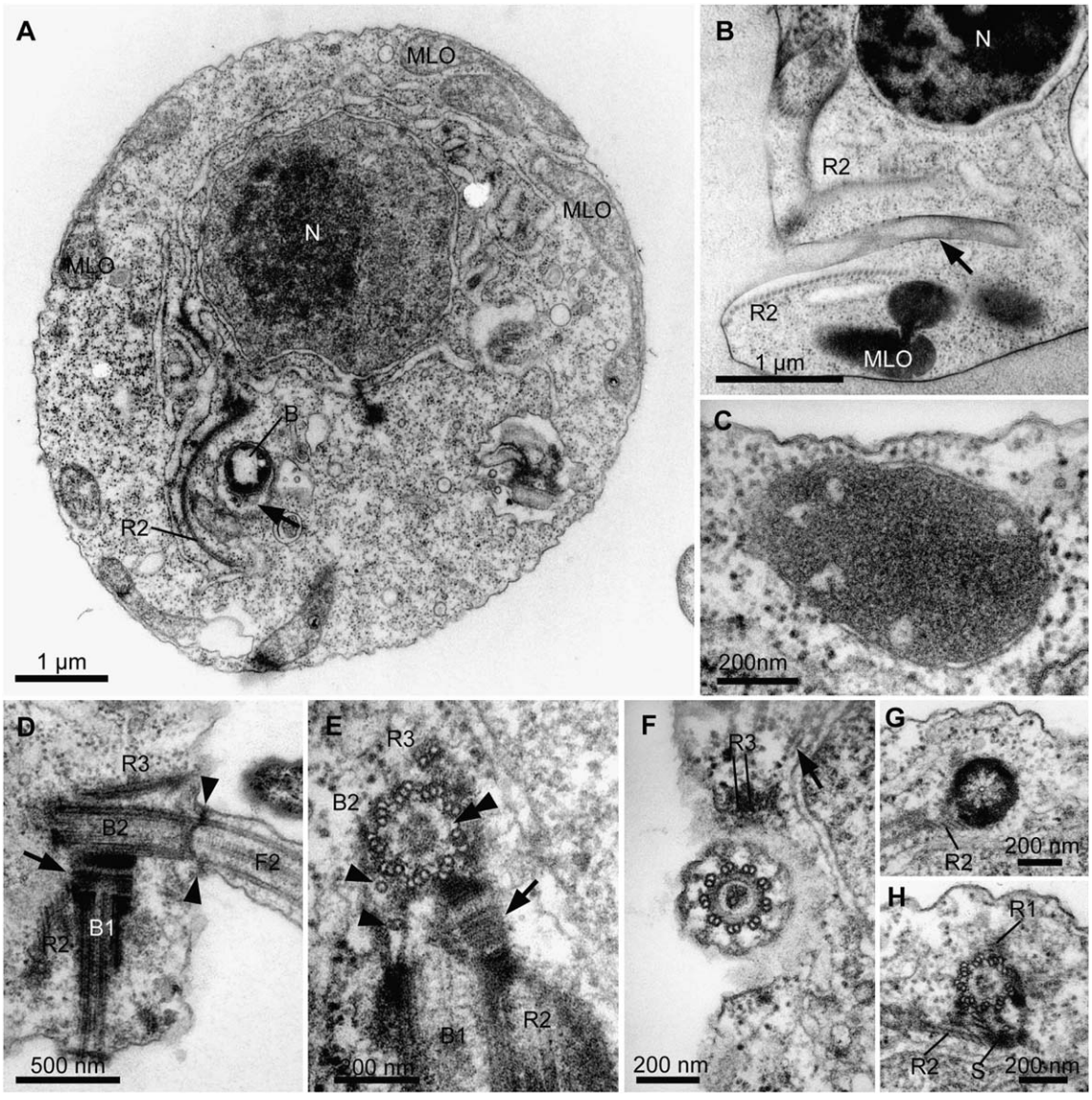

Figure 3. Transmission electron micrographs (TEM) showing the general ultrastructure of *Rictus lutensis* gen. et sp. nov. **A**. Low magnification view of a cross section through the cell body. The network of ER is well developed. A bacterium (B) is embedded within the cytopharynx (arrow), which is surrounded by the array microtubules derived from root 2 (R2). The mitochondria-like organelles (MLO) are located just under the cell membrane **B.** Longitudinal section through the cytopharynx (arrow) on the ventral side of the cell. The cytopharynx is surrounded by an array of microtubules designated as root 2 (R2). The cell in this section was prepared for TEM by high-pressure freezing. **C.** Cross section of a mitochondra-like organelle (MLO) bounded by two membranes and containing a sparse number of cristae. **D.** A longitudinal section of both basal body 2 (B2) and flagellum 2 (F2), and tangential section of basal body 1 (B1). A striated fiber (arrow) connects B2 and the dorsal side of B1. Arrowheads show the level of the section of image F. This section was viewed from the ventral side of the cell. **E.** Cross section of B2 viewed from the distal end of flagellum; the longitudinal section of B1 is observed from its left side. The striated fiber (arrow) connects the posterio-dorsal side of B2 and the dorsal side of B1. Two microtubules are positioned between the basal bodies (arrowheads). Double arrowheads indicate the intrakinetosomal shelf. **F.** Cross section of F2 viewed from the distal end of flagellum. The concentric ring in the axoneme is the edge of the concave transitional plate shown in D. Arrow shows the cytoplasmic microtubule emanating from R3. **G.** A cross section through the proximal level of B1 showing the electron dense material around the basal body and a cartwheel structure in B1. **H.** A cross section through B1 showing the fibers extending from the c tubule of the four triplets of B1.

the plasma membrane (Fig. 4F-K). The 'c' microtubule also possessed connective bands that bridged the x fiber and the S tubule (Fig. 4L). The 'abc' microtubules ran from the left posterior side of the cell in parallel with the S tubule and R1 and supported the left side of the cytostome.

The long arm of the L shape of R2 extended to the posterior end of the cell running adjacent to the nucleus. As this array of microtubules ran posteriorly, additional microtubules were added on the side of microtubule 7 and accumulated upwards of 50 microtubules at the loop region (Fig. 4D-J). Fine crosshatched fibers were associated with the left side of the microtubular array (Fig. 4D-F). After the microtubules passed along the side of the nucleus, an electron dense ribbon extended from the right side of the microtubules (Figs 4J and 5D-F). The row of microtubules turned counter-clockwise to form a loop along the periphery of the cytostome and headed back to the basal body along the right side of the 'abc' microtubules. As a whole, the R2 array of microtubules was shaped like a horseshoe. The cytopharynx was positioned inside the loop and

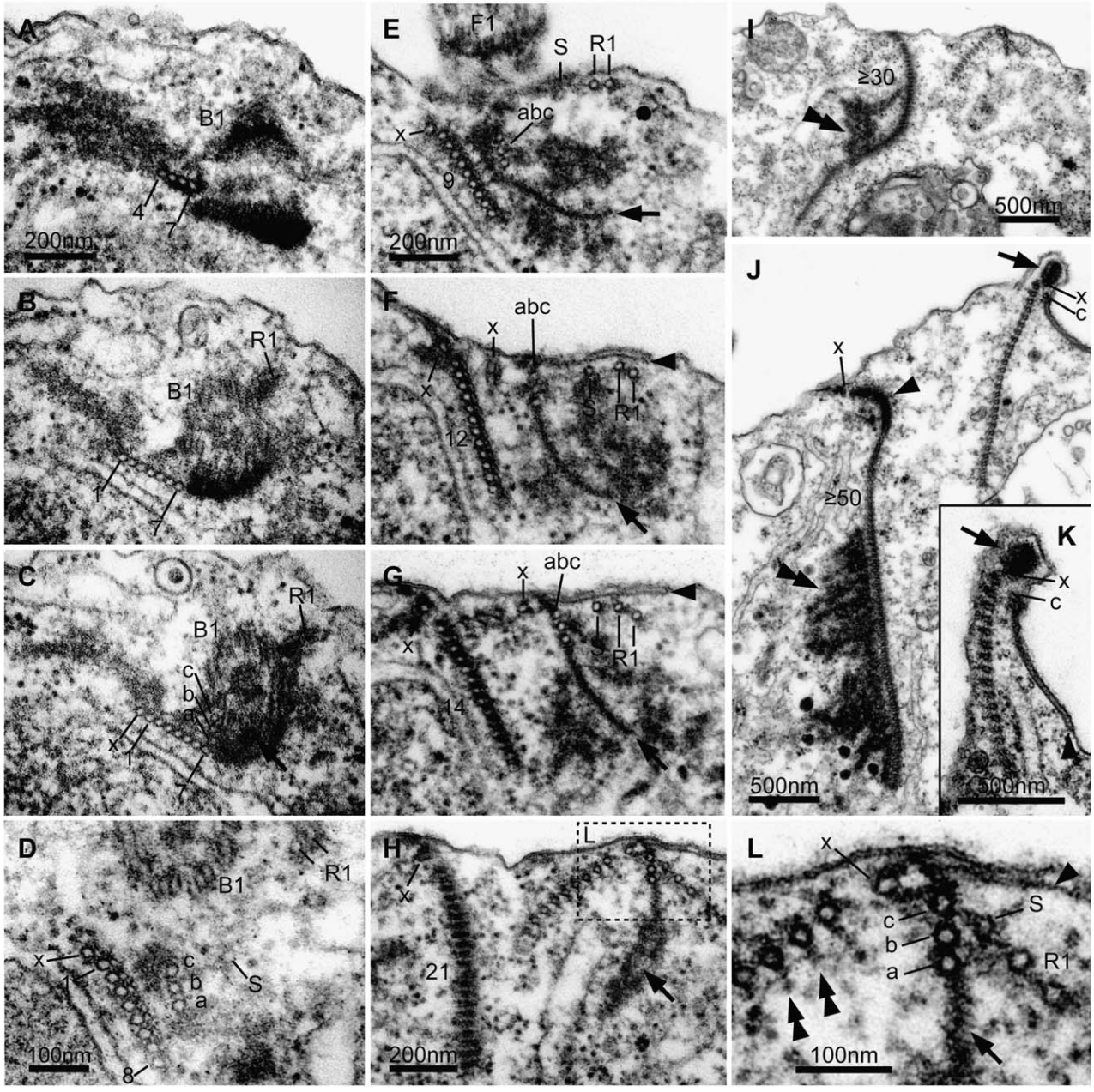

electron dense globules were sandwiched between the array of microtubules and the ER at the outside of the loop (Fig. 5C, F). The upper 10 to 15 microtubules close to the cytostome were embedded with an electron dense material (Figs 4J and 5A). The number of microtubules decreased as they moved back to the space between the 'abc' microtubules and the origin of the R2 array of microtubules. Distinct comb-like projections linked each returning microtubule with neighboring microtubules (Fig. 4L).

The x fiber was distinguishable from other microtubules by a small gap and by running outside of microtubule 1 for its entire distance. The left side of the cytostome was supported by an electron dense rod and the x fiber ran along the bottom of the rod on the way back to the basal body area (Fig. 4J, K). The returning x fiber linked the 'c' microtubule to a connective band (Fig. 4L).

Root 3 (R3): R3 was composed of two microtubules and extended from the anterior part of B2 (Fig. 3D-F). All of the cytoplasmic microtubules extended from R3. Two microtubules were positioned at the posterior side of B2. Both were shorter than the length of the basal body (Fig. 3E), and these (likely) become R2 and the S tubules in the next generation.

A illustration showing our reconstruction of the overall flagellar apparatus of *R. lutensis* gen. et sp. nov. is shown in Figure 6.

Phylogenetic Position of *Rictus lutensis* gen. et sp. nov.

We sequenced almost the entire length of the SSU rRNA gene (1789 bp) from *R. lutensis* and evaluated its phylogenetic position. The *R. lutensis* SSU robustly branched within stramenopiles in a preliminary tree that included the breadth of eukaryote diversity (data not shown). This is consistent with its highest BLASTn hit being *Blastocystis*. In Maximum Likelihood (ML) and Bayesian inference (BI) of a 100-taxon data set, containing the known diversity of stramenopile SSU sequences, *R. lutensis* robustly grouped with heterotrophic stramenopiles (Fig. 7). Optimal trees recovered a very weakly supported association of *R. lutensis* with a marine environmental SSU sequence obtained from the anoxic water column of Framvaren Fjord, Norway (SA1_1E06, EF526979, T. Stoeck personal communication).

Figure 4. Transmission electron micrographs (TEM) showing the flagellar apparatus of *Rictus lutensis* gen. et sp. nov., focusing on the orientation of root 1 (R1), the S tubule (S) and root 2 (R2). All sections are viewed from the posterior side of the cell. The section of A is closest to the basal bodies, and sections J and K are the farthest from the basal bodies. **A-C**; Non-consecutive serial sections. The scale of A is applicable for B-C. **A.** A section through the proximal part of B1. Four microtubules of R2 are seen at the posterior side of B1. **B.** Seven microtubules of R2. **C.** The x fiber is added onto microtubule 1 of R2. The 'abc' microtubules of the R2 appear on the ventral side of microtubule 7 forming an L shaped arrangement. The arrow indicates the S tubule. **D.** Higher magnification of the section showing R1, the S tubule (S) and R2. One microtubule is added on the side of the microtubule 7 of R2. The long part of R2 has crosshatched fibers on the left side. **E-I**; Non-consecutive serial sections. The scale of E is applicable for F-G. **E.** Nine microtubules are on the long part of R2. The S tubule (S) runs under the cell membrane in parallel with R1. The arrow indicates the sheet structure from the 'abc' microtubules. **F.** Twelve microtubules are shown as an array of microtubules stemming from R2. A thin layer (arrowhead) extends from the 'c' tubule of the 'abc' microtubules of R2, and a sheet structure (arrow) extends from the 'a' tubule of the 'abc' microtubules. An 'x fiber' is positioned between the array of 12 microtubules and the 'abc' microtubules. **G.** Fourteen microtubules form an array of microtubules from R2. Three microtubules are seen beside the returning x fiber. The arrow and arrowhead indicate the sheet structure from the 'a' tubule and the thin layer from the 'c' tubule, respectively. **H.** Twenty-one microtubules form an array of microtubules from R2. High magnification of dotted box is demonstrated in L. The arrow shows the sheet structure from the 'a' tubule. **I.** The double arrowhead indicates a ribbon extending from the right side of the array from R2. Thirty or more microtubules form an array of microtubules from R2. **J.** A dense rod (arrow) supports the left lip of the cytostome. The double arrowhead indicates the ribbon that extends from the right side of the array of microtubules from R2. Fifty or more microtubules form an array of microtubules from R2. The upper part of the microtubules are embedded in an electron dense structure (arrowhead). **K.** High magnification view of the left edge of the cytostome. The x fiber is near the bottom of the dense rod (arrow). The 'c' tubule is clearly associated with the thin layer (arrowhead). **L**. High magnification view of the dotted box shown in H. R1, the S tubule (S), the 'abc' microtubules, and the x fiber (x) are linked by the connective band. The sheet structure (arrow) and the thin layer (arrowhead) are from 'a' tubule and 'c' tubule, respectively. The comb-like projection (double arrowheads) is seen on the left side of R2.

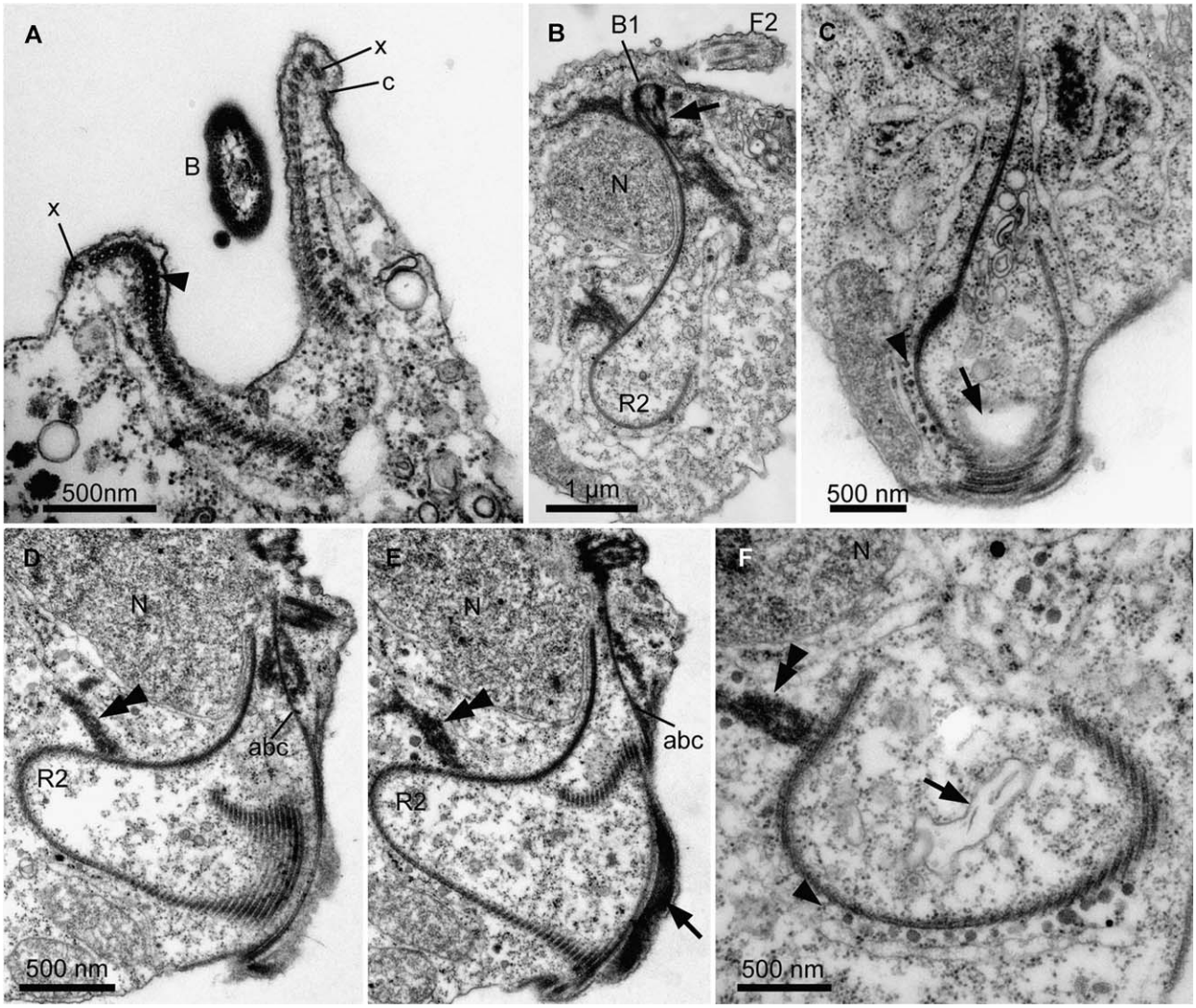

Figure 5. Transmission electron micrographs (TEM) of the flagellar apparatus of *Rictus lutensis* gen. et sp. nov. showing the organization of root 2 (R2). **A.** A cross section showing that the cytostome is supported by an array of microtubules derived from R2. A bacterial cell (B) is embedded in the cytostome. The upper part of the microtubules from R2 are embedded in an electron dense structure (arrowhead). **B.** R2 running along the side of nucleus. Four dense bands (arrow) extend from B1. **C.** R2 turns around the cytopharynx (arrow). The arrowhead indicates the small globules along R2. **D.** TEM showing that R2 heads back to the basal body area. The double arrowhead points to the ribbon from the right side of R2. **E.** A serial section with D showing the dense rod on the left lip of the cytosome (arrow). The double arrowhead indicates the ribbon from the right side of R2. **F.** The cytopharynx (arrow) is surrounded by the array of microtubules from R2. Small globules are located outside of the microtubular loop formed by R2 (arrowhead). The double arrowhead indicates the ribbon from the right side of the R2.

Both of these sequences were sister to the remaining bicosoecids. The bootstrap support value (BS=55) and the BI posterior probability (PP=0.97) for this position were relatively low. There was little support for a more specific phylogenetic affinity (such as within the Bicosoecida or other heterotrophic lineages). However, the SSU rDNA of *R. lutensis* is fairly divergent as evidenced by its long-branch in phylogenetic trees (Fig. 7, Supplementary Fig. S1). *R. lutensis* does not group with any described MAST clade, including MAST-9 and MAST-12, that probably represent anaerobic or anoxic-tolerant organisms.

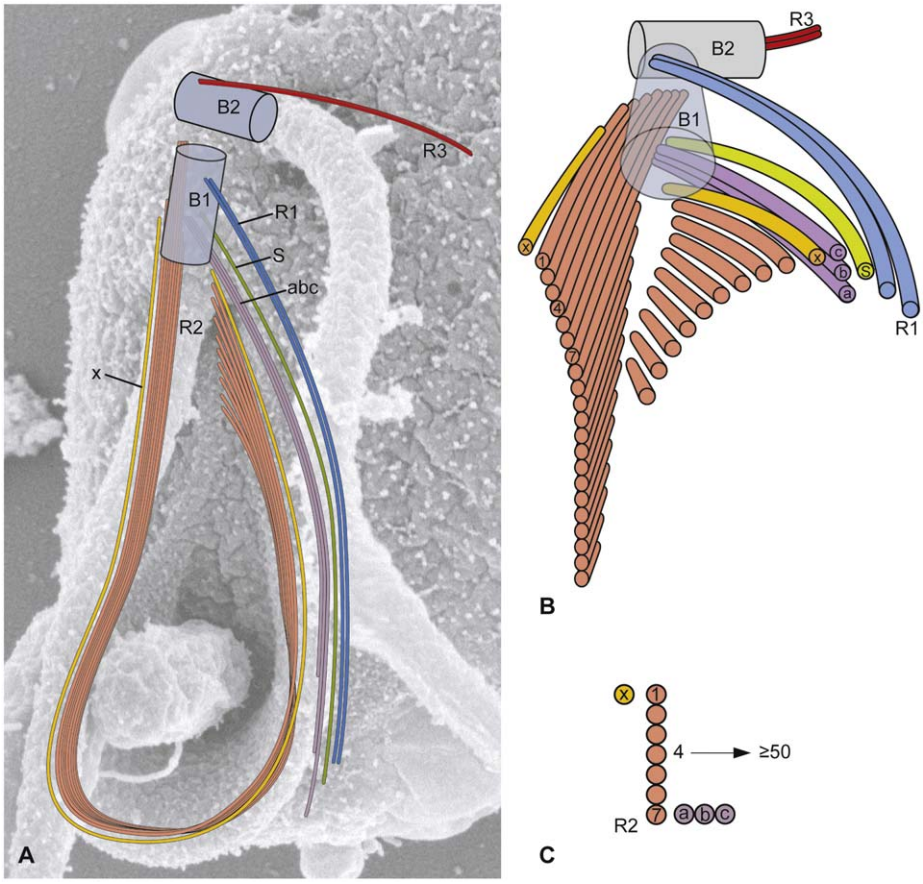

Figure 6. The diagram of flagellar apparatus of *Rictus lutensis* reconstructed from ultra-thin serial sections. **A**. Illustration of the flagellar apparatus superimposed on the scanning electron micrograph shown in Figure 2B and viewed from ventral side of the cell. Only nine microtubules of the long arm of R2 are depicted and fibrous structures are not shown on this diagram for clarity**. B.** The proximal area of the flagellar apparatus. The microtubular root systems was omitted at the level of the section shown in Figure 4H. abc; abc microtubules, s; the s tubule, R1-4; root 1-4, x; the x fiber. **C.** The L shape arrangement of R2 including the x fiber (x), abc microtubules (abc) and the array of mictorubules.

Finer scale analyses limited to the diversity of SSU sequences branching around Bicosoecida and Slopalina with Oomycetes and relatives serving as outgroups recovered a more strongly supported sister relationship between *R. lutensis*+SA1_1E06 and the remaining bicosoecids (82/1.0 BS/BI support respectively, Supplementary Fig. S1).

Discussion

Rictus lutensis gen. et sp. nov. is a Novel Lineage of Bicosoecids

Although our molecular phylogenetic analyses invariably placed *R. lutensis* in a clade with bicosoecids, the trees did not show robust support for this position. The ultrastructural features described here, however, are concordant with the molecular phylogenetic analyses; the L shaped arrangement of R2 in *R. lutensis*, and its involvement in food capture, is the hallmark for the bicosoecid clade (Karpov 2000; Karpov et al. 2001). In most bicosoecids, R2 is composed of an 8+3 (abc)+1 (x) arrangement of microtubules; some variations on this specific arrangement have been reported previously (e.g. *Siluania* and *Symbiomonas*) (Guillou et al. 1999; Karpov et al. 1998). The microtubules of R2 in *R. lutensis* constantly increase in number on both sides of the long arm of the L shape arrangement (perhaps over 50 microtubules are present). Accordingly, it is difficult to designate a specific number of microtubules associated with the L shape arrangement

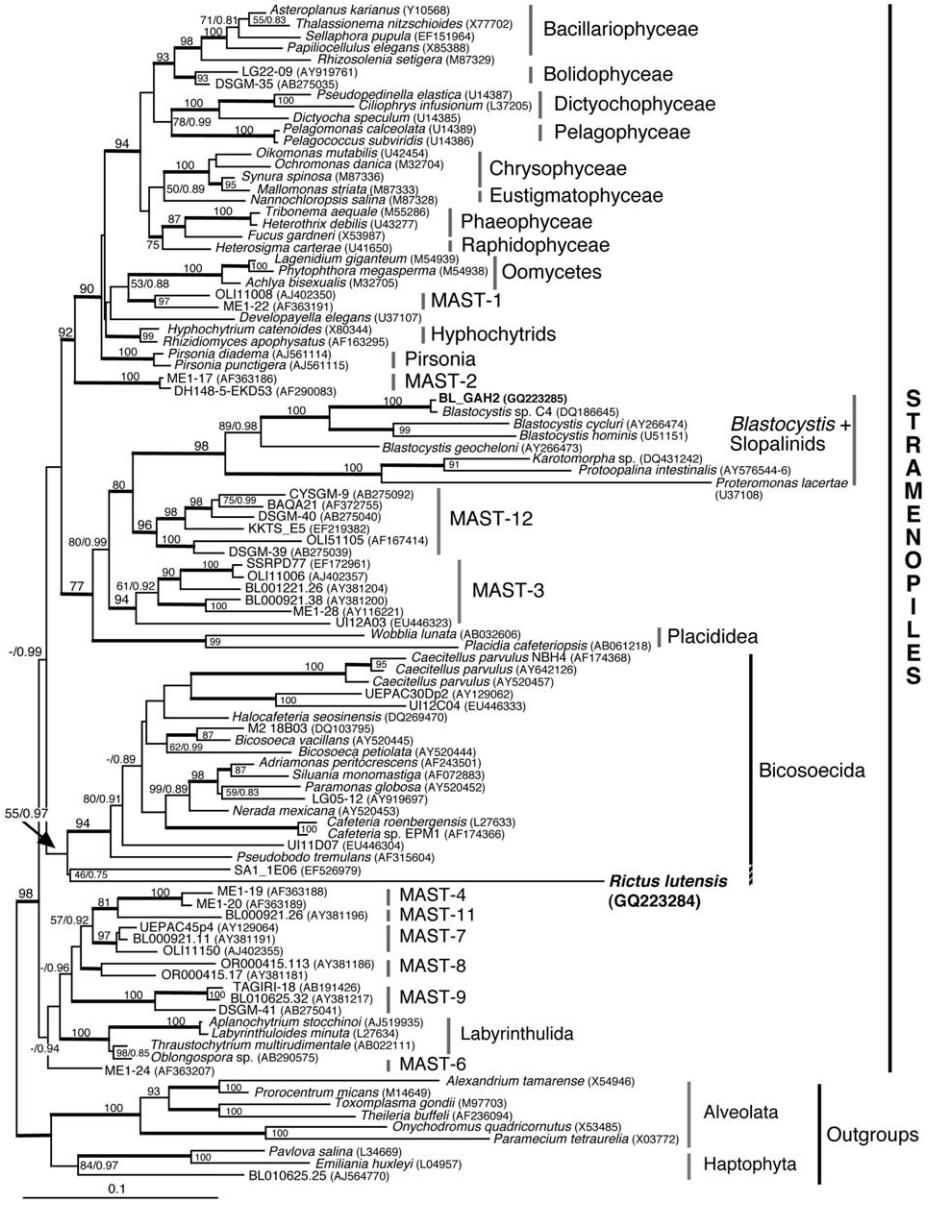

Figure 7. Phylogenetic tree inferred from 100 SSU rRNA sequences. The tree was inferred by the Maximum Likelihood (ML) method using a GTR+Γ+I model. ML bootstrap values over 50 and Bayesian posterior probabilities (PP) over 0.80 are shown at the nodes (except at the *R. lutensis* node, where all support values are shown). Instead of numbers, Bayesian PP=1.00 are represented by thick lines. Where two support values are displayed they represent ML bootstrap/Bayesian PP values respectively. *Rictus lutensis* and the new *Blastocystis* are highlighted in bold text. GenBank accession numbers follow each taxon name. The scale bar represents inferred evolutionary distance in changes/site. The minus sign (−): ML bootstrap values <50.

of R2 in *R. lutensis*. Nonetheless, the number of microtubules in both R1 and R3 of *R. lutensis* corresponds exactly to that of other bicosoecids.

The Bicosoecida is composed of four families that have been established using a combination of morphological characteristics associated with the lorica, body scales, and the cytopharynx: the Bicosoecidae, Siluaniidae, Cafeteriidae and Pseudodendromonadidae (Karpov 2000; Karpov et al. 2001). Based on Karpov's classification (2000), the morphology of *R. lutensis* is most similar to three species of Siluaniidae: *Siluania monomastiga*, *Adriamonas peritocrescens* and *Caecitellus parvulus*. All four species lack cell surface ornamentation

(e.g., a lorica or body scales) and have a permanent cytopharynx (Karpov 2000; Karpov et al. 1998; O'Kelly and Nerad 1998; Verhagen et al. 1994).

Siluania monomastiga and *A. peritocrescens* resemble one another in having a spiral fiber under the basal body transitional plate, which is absent from *R. lutensis* (Karpov et al. 1998, 2001). The R2 of *S. monomastiga* consists of a 3+1 arrangement and has fewer microtubules then *R. lutensis* and other bicosoecids (Karpov et al. 1998). The R2 of *A. peritocrescens* is also different from that in *R. lutensis* and consists of 11-12 microtubules (Verhagen et al. 1994). *A. peritocrescens* is also the only previously described species within the Siluaniidae that contains extrusomes; a feature not present in *R. lutensis*. The R2 of *C. parvulus*, by contrast, has the standard bicosoecid 8+3+1 organization, and microtubules are added to the end of the R2 array much like that observed here in *R. lutensis.* However, unlike that of *R. lutensis,* the R2 of *C. parvulus* is not arranged in a horseshoe shape and does not return to the basal body area. Only the x fiber joins the 'c' microtubule at the left side of basal body 1. Therefore, although some morphological features of *R. lutensis* are somewhat similar to some of the three previously described siluaniid genera (Karpov 2000), several other features of *R. lutensis* preclude its inclusion into any one of them.

The key synapomorphy for inclusion within the genus *Bicosoeca* is the presence of a lorica. Although *R. lutensis* lacks this feature, the overall morphology of the cell suggests that a comparison to *B. maris* is warranted (Moestrup and Thomsen 1976). For instance, the S tubule morphology of *R. lutensis* is most similar to that described in *B. maris*, which is different from the standard morphology seen in other bicosoecids and stramenopiles as whole (Karpov 2000). In both *B. maris* and *R. lutensis,* the S tubule originates near the 'abc' microtubules; however unlike *R. lutensis*, the S tubule (and R1) of *B. maris* does not support the cytostome lip. The R2 microtubules of both *B. maris* and *R. lutensis* are in an L shaped arrangement and additional microtubules are added to their long arm. In cross section, the cytopharynx is supported by a large number of microtubules near the posterior side of the cell. The array of the R2 microtubules in *B. maris*, however, does not return to the basal bodies in a horseshoe shape along the side of 'abc' microtubules.

Even though some environmental SSU sequences generated from samples collected in anoxic environments branch within Bicosoecida (i.e., clones UI12C04, M2 18B03, Alexander et al. 2009; Zuendorf et al. 2006; Fig. 7), most known bicosoecids thrive in aerobic environments and possess well-developed mitochondria. However, the flagellate *Cafeteria marsupialis* lives in anaerobic environments much like the one *R. lutensis* was collected from (Larsen and Patterson 1990; Lee and Patterson 2000; Lee et al. 2003). The overall cell morphology of both *R. lutensis* and *C. marsupialis* is also similar in being "D-shaped" in lateral view. However, *C. marsupialis* can be easily distinguished from *R. lutensis* by comparing the size of the cell, the length of the flagella and associated ornamentation, and the way the cell attaches to the substrate. The cells of *C. marsupialis* are larger than those of *R. lutensis*, and unlike *R. lutensis*, both flagella in *C. marsupialis* are about same length as the cell. Moreover, when feeding on bacteria, *C. marsupialis* attaches to the substrate with the distal tip of the posterior flagellum. Water currents are created towards the cell body by the anterior flagellum and environmental bacteria are drawn towards the ventral side of the cell where the cytostome is located. By contrast, *R. lutensis* does not use F1 as an anchor and does not create backwards directed water currents because this organism lacks mastigonemes.

Overall, the comparative ultrastructural data and molecular phylogenetic analyses reported here demonstrate that *R. lutensis* is a novel bicosoecid without clear affinities to any of the currently recognized subclades (i.e., taxa) within the group. This novel isolate also represents one of the few known bicosoecids described from low oxygen environments. We anticipate that an improved understanding of bicosoecid biodiversity will continue to shed considerable light on the ecological significance and biogeographical distributions of tiny heterotrophic microeukaryotes in marine benthic environments across the globe.

Taxonomic Summary

Stramenopile Patterson, 1989
Bicosoecida (Grassé) Karpov, 1998

Rictus gen. nov. Yubuki, Leander et Silberman

Description: cells with two heterodynamic flagella without mastigonemes. Conspicuous cytostome and cytopharynx supported by root 1, an S tubule

and a horseshoe-shaped root 2. Root 2 is L-shape at the origin. No lorica, body scales or extrusomes.

Type species: *Rictus lutensis*

Etymology: Rictus='opened mouth' in Latin

Rictus lutensis sp. nov. Yubuki, Leander et Silberman

Description: Spherical or D shaped cells with flagella of unequal length. Both flagella acronematic. Cells 6.8 μm (5.2-8.7 μm) long and 6.0 μm (4.4-8.5 μm) wide. Mitochondria-like organelles (MLO) distributed superficially beneath the plasma membrane and with reduced cristae. Found in low oxygen environments.

Holotype: Cryopreserved culture in ATCC.

Type locality: Prince Cove, Marstons Mills, MA, USA (Cape Cod, latitude=N41° 38′ 29″ longitude=W70° 24′ 48″)

Figure: Figure 1

Etymology: lutensis='mud dwelling' in Latin

Concluding Remarks

Phylogenetic analyses of SSU rRNA gene sequences suggest, albeit only modestly, that *R. lutensis* groups with bicosoecids. The SSU sequence from this flagellate does not cluster specifically with any DNA sequence clades composed entirely of uncultured/unidentified stramenopiles, such as the MAST clades representing diverse lineages recovered from low oxygen environments (i.e., "marine stramenopile" clades 1-12). We classified this organism as a member of Bicosoecida, because *Rictus* shared hallmark ultrastructural characters with Bicosoecida, such as the L shape arrangement of R2 involved in food capturing. Ultrastructural studies have generally been neglected, as molecular phylogenetic techniques have become the conventional approach for inferring the evolutionary relationships of microeukaryotes. This trend is concerning because the ultrastructural data reported here provide the most compelling evidence for inferring that *R. lutensis* is a member of the Bicosoecida; the SSU rDNA sequence data provided only weak evidence (that may be influenced by long branch attraction). Our sequence data, however, indicate that available environmental DNA surveys do not account for the full diversity of stramenopiles living in low oxygen environments, making investigations like ours necessary for improving the overall understanding of these ubiquitous flagellates.

Methods

Sampling and culture conditions: Soft mud samples were collected in sterile 50 ml polypropylene conical tubes on December 29, 2006 from coastal estuarian sediments of Prince Cove, Marstons Mills MA, USA. Sediment samples ~2-4 cm deep were collected at low tide under 2-3 inches of water (salinity=26 ppt). Each tube was approximately half full of sediment with the remainder of the tube filled to the top with seawater. The sediments had a distinct, sulfuric/anaerobic smell. Tightly sealed tubes were transported to the lab in Arkansas and ~1 ml of sediments were inoculated into various media in sealed 15 ml polypropylene tubes within 48 h of collection and maintained at room temperature (~21 °C). *Rictus lutensis* grew to high density in bi-phasic medium consisting of a solid slant of 3 ml inspissated horse serum (75-80 °C for 1.5 h) with 3 ml liquid overlay of natural seawater grass infusion (ATCC medium 1525 made with natural seawater at 26-35 ppt). A mono-eukaryotic culture was established by limiting dilution. The culture has been maintained by serial passage of ~0.5 ml into the bi-phasic medium (described above) pre-bacterized with *Klebsiella pneumoniae* (ATCC 23432) and monitored for anaerobic conditions using the color signal of rezasurin. The culture grows equally well at room temperature (~21 °C) to 14 °C. Weekly passage is required for cultures kept at room temperature. We maintain the culture at 14 °C in the dark with passages every 2-3 weeks. A viable frozen stock in 7% DMSO is also stored in liquid nitrogen at the University of Arkansas. *Rictus lutensis* has been deposited at the American Type Culture Collection (ATCC), Manasas VA, USA.

Light and electron microscopy: Light microscopy was performed using a Zeiss Axioplan 2 imaging microscope equipped with a Leica DC500 digital camera.

For Scanning electron microscopy (SEM), cells of *Rictus lutensis* were mixed with an equal volume of fixative containing 2% (v/v) glutaraldehyde and 0.2% (w/v) osmium tetroxide in 0.2 M sodium cacodylate buffer (SCB) (pH 7.2) and mounted on glass plates coated with poly-L-lysine at room temperature for 1.5 h. The glass plates were rinsed with 0.2 M SCB and fixed in 1% OsO_4 for 1 h. The fixed cells were then rinsed with 0.1 M SCB and dehydrated with a graded ethanol series from 30% to absolute ethanol. Samples were critical point dried with CO_2 using a Tousimis Critical Point Dryer. Samples were then coated with gold using a Cressington 208HR high Resolution Sputter Coater, and observed with a Hitachi S-4700 field emission scanning electron microscope.

Negatively stained specimen was prepared by mixing cell suspensions with an equal volume of fixative containing 5% (v/v) glutaraldehyde and 0.2 M sucrose in 0.2 M cacodylate buffer (pH 7.2). A drop of the specimen was put onto formvar-coated grids. After 10 min, liquid was removed and a drop of 2% uranyl acetate was placed on the grid for 2 min. Before drying the sample, liquid was removed with filter paper.

For ultra-thin section, cell suspensions were mixed with 2% (v/v) glutaraldehyde and 0.2% (w/v) osmium tetroxide in 0.2 M cacodylate buffer (pH 7.2) at 4 °C for 30 min. Cells were aggregated into a pellet by centrifugation at 750 rcf for 5 min and then rinsed with 0.2 M SCB (pH 7.2). The specimens were then fixed in 1% (w/v) osmium tetroxide in 0.2 M SCB (pH 7.2) at room temperature for one hour followed by dehydration through an ethanol series, and substitution with Acetone. The specimens were embedded in resin (Epon 812).

For Figure 3B, cells were high-pressure frozen using the Leica HPM100. Cells were freeze-substituted in 1% osmium

tetroxide and 0.1% uranyl acetate in HPLC grade acetone using the Leica AFS set to −85 °C for 5 days, warming to −20 °C over 13 h and held at −20 °C for 6 h before warming to room temperature over 14 h. The cells were washed in fresh HPLC grade acetone, and then increasing concentrations of a 1:1 mixture of JEMBED and Spurr's resin diluted with HPLC grade acetone was infiltrated using the Pelco 3450 laboratory microwave set to 300 W for 3 min with 20 inches of mercury vacuum applied to the cells. The microwave infiltration of 100% resin was supplemented with extended periods of room temperature mixing on a rotator. The infiltrated samples were polymerized overnight in fresh 1:1 JEMBED:Spurr's resin at 60 °C. Ultra-thin sections were cut on an Leica EM UC6 ultramicrotome and double stained with 2% (w/v) uranyl acetate and lead citrate (Reynolds 1963). Negatively stained specimen and ultra-thin sections were observed using a Hitachi H7600 electron microscope.

DNA extraction, PCR amplification, alignment and phylogenetic analysis: Actively growing cells were pelleted at 3000 rcf for 10 min at 4 °C. The supernatant was removed and genomic DNA isolated from the cell pellet (consisting of the protist plus bacterial food) using the PureGene tissue DNA isolation kit (Qiagen, Valencia CA). The nearly complete nuclear small subunit ribosomal RNA gene (SSU) was amplified by polymerase chain reaction (PCR) in a 20 μl reaction volume using the 'universal' eukaryotic SSU primers "A" and "B" (Medlin et al. 1988), GoTaq Green master mix (Promega, Madison WI) and 100 ng template DNA with the following cycling parameters: initial denaturation at 94 °C for 45 s followed by 33 cycles of 25 s denaturation at 94 °C, 1 min annealing at 42 °C, and elongation at 72 °C for 3 min, yielding a single amplicon of ~1.9 kb. The SSU was T/A cloned into pCR4-TOPO (Invitrogen, Carlsbad CA) and 10 clones were pooled and sequenced completely on both strands. PCR, cloning and sequencing were performed twice independently on DNA isolated 6 months apart. The *R. lutensis* sequences from these PCRs were identical. To increase stramenopile SSU diversity, a *Blastocystis* 'environmental' SSU sequence was generated from an early passage (P2) enrichment culture initiated from freshwater sediments from a local Fayetteville AR stream (same bi-phasic medium as above except the liquid overlay was freshwater grass infusion, ATCC medium 802). DNA isolation and PCR was as described above, except a single SSU clone was sequenced. These sequences are accession in GenBank, GQ223284 – GQ223285.

The new SSU gene sequences were laced into a preexisting alignment containing representatives of most major eukaryotic lineages. A preliminary Maximum Likelihood (ML) analysis of an 117 taxon data set showed that *R. lutensis* branched within the stramenopile lineage. Therefore an 100 taxon SSU data set comprising the known diversity of stramenopiles, including the rich diversity uncovered from environmental sampling was compiled with alveolates and haptophytes as outgroups. Phylogenetic analyses were based on 1433 unambigiously aligned positions. Maximum likelihood and Bayesian inferences (BI) trees were built under a GTR+Γ+I model as suggested by all criteria implemented in jModelTest v0.1.1 (Posada 2008). ML analyses were run in RAxML v7.0.4 (Stamatakis 2006) utilizing 30 discrete rate categories to describe among-site rate heterogeneity. All remaining parameters were estimated during the analyses (GTRMIX model). Bayesian inferences implemented 8 discrete rate categories for describing among-site rate heterogeneity.

Bayesian analyses run in MrBayes v3.12 (Ronquist and Huelsenbeck 2003; Altekar et al. 2004) consisted of two independent Markov chain Monte Carlo (MCMC) runs of 15×10^6 generations printing trees every 100 generations with a burnin of 12.4×10^6 generations by which time all parameters converged as assessed by an average standard split deviation that hovered around 0.0032 and the potential scale reduction factor=1.0 for all parameters. All BI analyses were carried out on the University of Oslo's Bioportal (www.bioportal.uio.no). Topological support was further assessed through 2000 bootstrap replicates in RAxML on the freely available CIPRES portal (www.phylo.org, Stamatakis et al. 2008). The ML bootstrap values were drawn onto the best-scoring tree of 500 RAxML tree searches (Fig. 7).

Acknowledgements

This work was supported by grants from the Tula Foundation (Centre for Microbial Diversity and Evolution), the National Science and Engineering Research Council of Canada (NSERC 283091-04) and the Canadian Institute for Advanced Research, Program in Integrated Microbial Biodiversity.

Appendix. Supplementary material

Supplementary data associated with this article can be found in the online version at doi:10.1016/j.protis.2009.10.004.

References

Alexander E, Stock A, Breiner HW, Behnke A, Bunge J, Yakimov MM, Stoeck T (2009) Microbial eukaryotes in the hypersaline anoxic L'Atalante deep-sea basin. Environ Microbiol **11**:360–381

Altekar G, Dwarkadas S, Huelsenbeck JP, Ronquist F (2004) Parallel Metropolis coupled Markov chain Monte Carlo for Bayesian phylogenetic inference. Bioinformatics **20**:407–415

Andersen RA (1987) Synurophyceae classis nov., a new class of algae. Am J Bot **74**:337–353

Andersen RA (1989) Absolute orientation of the flagellar apparatus of *Hibberdia magna* comb. nov. (Chrysophyceae). Nord J Bot **8**:653–669

Andersen RA (1991) The cytoskeleton of chromophyte algae. Protoplasma **164**:143–159

Andersen RA (2004) Biology and systematics of heterokont and haptophyte algae. Am J Bot **91**:1508–1522

Andersen RA, Saunders WG, Paskind MP, Sexton JP (1993) Ultrastructure and 18S rRNA gene sequence for *Pelagomonas calceolata* gen. et sp. nov. and the description of a new algal class, the Pelagophyceae Classis nov. J Phycol **29**:701–715

Archibald JM (2009) The puzzle of plastid evolution. Curr Biol **19**:R81–R88

Arisue N, Hashimoto T, Yoshikawa H, Nakamura Y, Nakamura G, Nakamura F, Yano TA, Hasegawa M (2002) Phylogenetic position of *Blastocystis hominis* and of stramenopiles inferred from multiple molecular sequence data. J Eukaryot Microbiol **49**:42–53

Barr DJS, Allan PME (1985) A comparision of the flagellar aparatus in *Phytophthora*, *Saprolegnia*, *Tharaustrochytrium*, and *Rhizidiomyces*. Can J Bot **63**:138–154

Behnke A, Bunge J, Barger K, Breiner HW, Alla V, Stoeck T (2006) Microeukaryote community patterns along an O_2/H_2S gradient in a supersulfidic anoxic fjord (Framvaren, Norway). Appl Environ Microbiol **72**:3626–3636

Ben Ali A, De Baere R, De Wachter R, Van de Peer Y (2002) Evolutionary relationships among heterokont algae (the autotrophic stramenopiles) based on combined analyses of small and large subunit ribosomal RNA. Protist **153**:123–132

Dick MW ed (2001) Including Accounts of the Marine Straminipilous Protists, the Plasmodiophorids, and Similar Organisms. Kluwer Academic Publishers, Dordrecht

Daugbjerg N, Andersen RA (1997) A molecular phylogeny of the heterokont algae based on analyses of chloroplast-encoded *rbcL* sequence data. J Phycol **33**:1031–1041

Fenchel T, Patterson DJ (1988) *Cafeteria roenbergensis*. nov. gen., nov. sp., a heterotrophic microflagellate from marine plankton. Mar Microb Food Webs **3**:9–19

Guillou L, Chretiennot-Dinet MJ, Boulben S, Moon-van der Staay SY, Vaulot D (1999) *Symbiomonas scintillans* gen. et sp. nov. and *Picophagus flagellatus* gen. et sp. nov. (Heterokonta): two new heterotrophic flagellates of picoplanktonic size. Protist **150**:383–398

Honda D, Yokochi T, Nakahara T, Raghukumar S, Nakagiri A, Schaumann K, Higashihara T (1999) Molecular phylogeny of labyrinthulids and thraustochytrids based on the sequencing of 18S ribosomal RNA gene. J Eukaryot Microbiol **46**:637–647

Karpov SA (2000) Ultrastructure of the aloricate bicosoecid *Pseudobodo tremulans*, with revision of the order Bicosoecida. Protistology **1**:101–109

Karpov SA, Kersanach R, Williams DM (1998) Ultrastructure and 18S rRNA gene sequence of a small heterotrophic flagellate *Siluania monomastiga* gen. et sp. nov. (Bicosoecida). Eur J Protistol **34**:415–425

Karpov SA, Sogin ML, Silberman JD (2001) Rootlet homology, taxonomy, and phylogeny of bicosoecids based on 18S rRNA gene sequences. Protistology **2**:34–47

Kostka M, Hampl V, Cepicka I, Flegr J (2004) Phylogenetic position of *Protoopalina intestinalis* based on SSU rRNA gene sequence. Mol Phylogenet Evol **33**:220–224

Kostka M, Cepicka I, Hampl V, Flegr J (2007) Phylogenetic position of *Karotomorpha* and paraphyly of Proteromonadidae. Mol Phylogenet Evol **43**:1167–1170

Larsen J, Patterson DJ (1990) Some flagellates (Protista) from tropical marine sediments. J Nat Hist **24**:801–937

Lee WJ, Patterson DJ (2000) Heterotrophic flagellates (Protist) from marine sediments of Botany Bay, Australia. J Nat Hist **34**:483–562

Lee WJ, Brandt SM, Vørs N, Patterson DJ (2003) Darwin's heterotrophic flagellates. Ophelia **57**:63–98

Leipe DD, Tong SM, Goggin CL, Slemenda SB, Pieniazek NJ, Sogin ML (1996) 16S-like rDNA sequences from *Developayella elegans*, *Labyrinthuloides haliotidis*, and *Proteromonas lacerate* confirm that the stramenopiles are a primarily heterotrophic group. Eur J Protistol **32**:449–458

Leipe DD, Wainright PO, Gunderson HJ, Poter D, Patterson DJ, Valois F, Himmerich S, Sogin ML (1994) The stramenopiles from a molecular perspective: 16S-like rRNA sequences from *Labyrinthula minuta* and *Cafeteria roenbergensis*. Phycologia **33**:369–377

Massana R, Castresana J, Balague V, Guillou L, Romari K, Groisillier A, Valentin K, Pedros-Alio C (2004) Phylogenetic and ecological analysis of novel marine stramenopiles. Appl Environ Microbiol **70**:3528–3534

Moestrup Ø (1982) Flagellar structure in algae: a review, with new observations particularly on the Chrysophyceae, Phaeophyceae (Fucophyceae), Euglenophyceae and *Reckertia*. Phycologia **21**:427–528

Moestrup Ø (2000) The Flagellate Cytoskeleton: Introduction of a General Terminology for Microtubular Flagellar Roots in Protists. In Leadbeater SC, Green JC (eds) The Flagellates Unity. Diversity and Evolution. Taylor & Francis Ltd, London, pp 69–94

Moestrup Ø, Thomsen HA (1976) Fine structural studies on the flagellate genus *Bicoeca*. I. *Bicoeca maris* with particular emphasis on the flagellar apparatus. Protistologica **12**:101–120

Moriya M, Nakayama T, Inouye I (2000) Ultrastructure and 18S rDNA sequence analysis of *Wobblia lunata* gen. et sp. nov., a new heterotrophic flagellate (Stramenopiles, Incertae sedis). Protist **151**:41–55

Moriya M, Nakayama T, Inouye I (2002) A new class of the stramenopiles, Placididea Classis nova: description of *Placidia cafeteriopsis* gen. et sp. nov. Protist **153**:143–156

O'Kelly CJ, Nerad TA (1998) Kinetid architecture and bicosoecid affinities of the marine heterotrophic nanoflagellate *Caecitellus parvulus* (Griessmann, 1913) Patterson et al., 1993. Eur J Protistol **34**:369–375

O'Kelly CJ, Patterson DJ (1996) The flagellar apparatus of *Cafeteria roenbergensis* Fenchel & Patterson, 1988 (Bicosoecales=Bicosoecida). Eur J Protistol **32**:216–226

Park JS, Cho BC, Simpson AGB (2006) *Halocafeteria seosinensis* gen. et sp. nov. (Bicosoecida), a halophilic bacterivorous nanoflagellate isolated from a solar saltern. Extremophiles **10**:493–504

Patterson DJ (1985) The fine structure of *Opalina ranarum* (family Opalinidae): Opalinid phylogeny and classification. Protistologica **21**:413–428

Patterson (1989) Stramenopiles: Chromophytes from a Protistan Perspective. In Green JC, Leadbeater BSC, Diver WI (eds) The Chromophyte Algae: Problems and Perspectives. Systematic Association Special, Vol. 38. Clarendon Press, Oxford, pp 357–379

Posada D (2008) ModelTest: Phylogenetic model averaging. Mol Biol Evol **25**:1253–1256

Reynolds ES (1963) The use of lead citrate at high pH as an electron-opaque stain in electron microscopy. J Cell Biol **17**:208–212

Riisberg I, Orr RJ, Kluge R, Shalchian-Tabrizi K, Bowers HA, Patil V, Edvardsen B, Jakobsen KS (2009) Seven Gene Phylogeny of Heterokonts. Protist **160**:191–204

Ronquist F, Huelsenbeck JP (2003) MRBAYES 3: Bayesian phylogenetic inference under mixed models. Bioinformatics **19**:1572–1574

Silberman JD, Sogin ML, Leipe DD, Clark CG (1996) Human parasite finds taxonomic home. Nature **380**:398

Stamatakis A (2006) RAxML-VI-HPC: Maximum likelihood-based phylogenetic analyses with thousands of taxa and mixed models. Bioinformatics **22**:2688–2690

Stamatakis A, Hoover P, Rougemont J (2008) A rapid bootstrap algorithm for the RAxML Web-servers. Syst Biol **75**:758–771

Takishita K, Yubuki N, Kakizoe N, Inagaki Y, Maruyama T (2007) Diversity of microbial eukaryotes in sediment at a deep-sea methane cold seep: surveys of ribosomal DNA libraries from raw sediment samples and two enrichment cultures. Extremophiles **11**:563–576

Teal TH, Guillemette T, Chapman M, Margulis L (1998) *Acronema sippewissettensis* gen. nov. sp. nov., microbial mat bicosoecid (Bicosoecales=Bicosoecida). Eur J Protistol **34**:402–414

Tong SM (1995) *Developayella elegans* nov. gen., nov. spec., a new type of heterotrophic flagellate from marine plankton. Eur J Protistol **31**:24–31

Tsui CK, Marshall W, Yokoyama R, Honda D, Lippmeier JC, Craven KD, Peterson PD, Berbee ML (2009) Labyrinthulomycetes phylogeny and its implications for the evolutionary loss of chloroplasts and gain of ectoplasmic gliding. Mol Phylogenet Evol **50**:129–140

Van de Peer Y, Van der Auwera G, De Wachter R (1996) The evolution of stramenopiles and alveolates as derived by "substitution rate calibration" of small ribosomal subunit RNA. J Mol Evol **42**:201–210

Verhagen FJM, Zölffel M, Brugerolle G, Patterson DJ (1994) *Adriamonas peristocrescens* gen. nov., sp. nov., a new free-living soil flagellate (Protista, Pseudodendromonadidae incertae sedis). Eur J Protistol **30**:295–308

Zuendorf A, Bunge J, Behnke A, Barger KJ, Stoeck T (2006) Diversity estimates of microeukaryotes below the chemocline of the anoxic Mariager Fjord, Denmark. FEMS Microbiol Ecol **58**:476–491